Contents lists available at ScienceDirect

Journal of Chromatography A

journal homepage: www.elsevier.com

Highly-porous diatom biosilica stationary phase for thin-layer chromatography

Joseph A. Kraai[a], Gregory L. Rorrer[a,*], Alan X. Wang[b]

[a] School of Chemical, Biological, and Environmental Engineering, Oregon State University, Corvallis, OR 97331, USA
[b] School of Electrical Engineering and Computer Science, Oregon State University, Corvallis, OR 97331, USA

ARTICLE INFO

Article history:
Received 1 November 2018
Received in revised form 10 January 2019
Accepted 12 January 2019
Available online xxx

Keywords:
Biosilica
Diatom
Nanostructured
Triphenylmethane dye
Thin-layer chromatography

ABSTRACT

This study showed that a nanostructured, highly-porous stationary phase composed of randomly-deposited biosilica frustules isolated from living cells of diatom *Pinnularia* sp. significantly improved the conventional thin-layer chromatography (TLC) based separation of the triphenylmethane dyes malachite green and fast green relative to silica gel by two mobile phases (9:1:1 v/v 1-butanol:ethanol:water, 5:1:2 v/v 1-butanol:acetic acid:water). Although both stationary phases were composed of amorphous silica rich in silanol groups with particle size of 10–12 μm, diatom biosilica frustules were highly porous, hollow shells with surface structure dominated by 200 nm pore arrays. Diatom biosilica significantly improved the mobility of both malachite green and fast green, enabling the resolution of these analytes. The diatom biosilica layer had a high void fraction of 96% but reduced the flow velocity and permeability constant by a factor of two relative to silica gel. TLC performance was enhanced, as evidenced by ten-fold reduction in theoretical plate height for both analytes using the 1-butanol:acetic acid:water mobile phase, and an increased difference in retention time between malachite green and fast green ($\Delta R_f = 0.26$) using the 1-butanol:ethanol:water mobile phase. Analysis of plate height vs. solvent front position by the modified van Deemter equation suggested that dispersive mass transfer was reduced, leading to improved analyte resolution, and that surface of the frustule decreased boundary layer resistance, leading to increased analyte flux. Overall, the basis for improved chromatographic performance is believed to be the unique nano- and microstructure of the diatom biosilica frustule.

1. Introduction

Thin-layer chromatography (TLC) is a versatile tool for analytical chemistry [1], and offers the widest range of stationary phases for separating various sample matrices of any liquid chromatographic method [2,3]. Advances in TLC have resulted from stationary phase improvements including pre-coated stationary phase layers [4], high-performance TLC [5], and ultra TLC, particularly for nanostructured silica-based materials [6–9].

In this study, thin porous layers comprised of intact *Pinnularia* sp. diatom biosilica frustules are introduced as new stationary phase for conventional TLC. Diatoms are single-celled algae that take up and biomineralize dissolved silicon in the form of $Si(OH)_4$ to biologically fabricate nano-patterned, micron-scale silica shells called frustules rich in silanol groups. The frustules are hollow with approximately 100 nm wall thickness, and consist of upper and lower halves. *Pinnularia* sp. diatoms have ellipsoidal frustules with minor axis of nominally 20 μm and major axis of 5–10 μm. Each shell contains a periodic rectangular array of 200 nm diameter pores penetrating fully through the shell, spaced approximately 300 nm apart [10]. In contrast, 10–12 μm silica gel particles for TLC possess a random, internal mesoporous structure with average pore size around 6 nm [11].

The overall goal of this study is to compare the TLC separation performance of porous, thin layers made of diatom biosilica frustules and silica gel particles of similar size. Some classes of molecules remain difficult to separate via TLC, such as highly-polar, ionic analytes, owing to their limited mobility on polar layers like silica gel [11,12]. Furthermore, a recognized issue with porous layers for conventional TLC is that capillary forces cannot generate sufficient flow to minimize the effects of zone broadening [1], and silica gel particle layers in particular suffer from inadequate mass transfer [13]. We hypothesize that the open, porous structure of the diatom biosilica frustules may promote local mobile phase interaction with the hydrated silica stationary phase, leading to improved mass transfer and chromatographic separation of these analytes. The nanostructure is provided by the diatom biosilica particle itself, whereas the microstructure is provided by the random packing of the ellipsoidal particles in the stationary phase.

The reference analytes chosen for this study are the triphenylmethane dyes malachite green and fast green FCF. Malachite green is relatively nonpolar and weakly cationic with two *N*-dimethyl groups, whereas fast green additionally possesses anionic benzene and phenol sulfonate groups (Fig. 1). Malachite green has been widely used to prevent and treat infections in aquaculture products, but has toxic effects on fish [14]. There is significant interest in the development of rapid and simple methods for the detection of malachite green in seafood products [15], and TLC is one simple method to enable the separation component of the detection platform. Planar

* Corresponding author.
Email address: gregory.rorrer@oregonstate.edu (G.L. Rorrer)

https://doi.org/10.1016/j.chroma.2019.01.037
0021-9673/

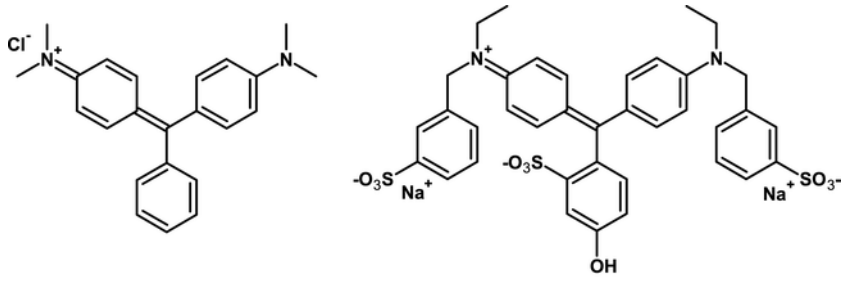

Malachite Green **Fast Green FCF**

Fig. 1. Molecular structures of malachite green and fast green.

chromatography on silica gel stationary phases has been used for analysis of triphenylmethane dyes, including malachite green and fast green, but not within the same sample matrix [16].

The TLC-based separation performance of malachite green and fast green on diatom biosilica and silica gel will be assessed through characterization of solvent migration front vs. time, analyte retention factor, and the height equivalent to a theoretical plate. We report that nanostructured diatom biosilica offers significant enhancements in performance for TLC-based separation of malachite green and fast green relative to on silica gel, and merits continued investigation as a stationary phase for TLC.

2. Materials and methods

2.1. Analytes and mobile phase

Malachite green chloride, $C_{23}H_{25}ClN_2$, mol. wt. 364.917 g/mol, CAS Number 569-64-2, was obtained from Sigma-Aldrich (38800, analytical standard grade, > 96% purity). Fast Green For Coloring Food (FCF), $C_{37}H_{34}N_2Na_2O_{10}S_3$, mol. wt. 808.843 g/mol, CAS Number 2353-45-9, was obtained from Glentham Life Sciences (42053). Two solvent systems known for separation of malachite green on silica gel [16,17], consisting of 9:1:1 (v/v/v) 1-butanol:ethanol:water (solvent system 1), and 5:1:2 (v/v/v) 1-butanol:acetic acid:water (solvent system 2) served as the mobile phases. All solvents were analytical grade purity.

2.2. Diatom cell culture

Diatom culturing methods were adapted from those previously described [18]. Axenic cultures of the photosynthetic marine pennate diatom *Pinnularia* sp. were obtained from the UTEX Culture Collection of Algae (UTEX #B679). Diatoms were cultivated in 500 mL foam-stoppered borosilicate flasks containing 100 mL of Harrison's Artificial Seawater Medium (ASM) with a modified Guillard's f/2 nutrient enrichment [19]. Culture flasks were incubated at 22 °C under a light intensity of 100 μE/m^2 s on a 14h:10 h light:dark photoperiod, and subcultured every 21 days at 10:1 dilution in fresh medium. Typical cell number density at cell harvest was 1×10^6 cells/mL. Cell number density of *Pinnularia* sp. culture was measured using a Beckman Coulter Z2 Particle Counter at a lower threshold of 6 μm using a 100 μL aliquot of the cell suspension diluted in 10 mL of diluent (10 g/L sterile-filtered NaCl, 171 mM).

2.3. Diatom biosilica frustule isolation

Intact biosilica frustules were isolated from *Pinnularia* sp. cell culture using an acidified hydrogen peroxide treatment method adapted from previous work [18]. Approximately 1200 mL of three week-old *Pinnularia* sp. flask cultures were pooled and allowed to settle. After decanting the majority of the cell-free supernatant, the cell density was measured, and a 120 mL aliquot of the concentrated cell suspension (~$3 \cdot 10^8$ cells) was centrifuged (20 min at 2500 *g*). The cell pellet was washed with 40 mL nanopure water three times to remove culture medium salts. The washed cell pellet was re-suspended in 15 mL of 8.1 M HCl in a 50 mL centrifuge tube, gently mixed by inverting five times, allowed to gravity settle, and the supernatant was pipetted out. In the first oxidation treatment, 5 mL of the concentrated slurry was added to 32 mL of 0.76 M HCl in 28% (v/v) H_2O_2, gently mixed by inverting the centrifuge tube five times, and then allowed to sit in an unsealed centrifuge tube for 72 h, with daily mixing via five inversions for the first two days. In the second oxidation treatment, this process was repeated. After removing the supernatant, the crude frustule isolate slurry was re-suspended in 40 mL H_2O and allowed to gravity settle, and then washed two additional times using 40 mL water. The supernatant was removed, and the washed frustule slurry was re-suspended in 40 mL anhydrous methanol (MeOH), allowed to gravity settle, and then washed two more times using 40 mL MeOH. The final frustule isolate was stored in MeOH suspension within a sealed centrifuge tube at room temperature. Frustule biosilica yield was typically 20 mg.

2.4. Fabrication of diatom biosilica and silica gel TLC stationary phases

Glass microscope slides (VWR, 75 × 25 mm, 1.0 mm thick) were cut into 75 × 3 mm substrates using a diamond-tipped scribe. Substrates were sonicated in a 1% (v/v) solution of Liquinox detergent for 60 min at 40 °C using a Branson model 2510 ultrasonic cleaner, rinsed with Nanopure H_2O and 100% ethanol (EtOH), dried under flowing nitrogen (N_2), cleaned in a Novascan PSD-UVT UV-ozone cleaner at 90 °C for 1 h, then stored in a desiccator until use.

Diatom biosilica porous layers were prepared by a drop-casting technique. Cleaned 75 × 3 mm glass substrates were placed on a hot plate surface at a temperature of 45 °C. Then, 100 μL of a 11.3 mg/mL *Pinnularia* sp. frustule suspension in methanol (MeOH) was evenly dispensed on the substrate surface. After evaporation of methanol (20–30 s), the dropcast diatom biosilica porous layers were treated in a UV-Ozone cleaner at 90 °C for 24 h to fix the frustule porous layer to the substrate surface and oxidize residual organic contaminants. The diatom biosilica layers were stored in a desiccator.

Silica gel porous layers on an aluminum backing were obtained from Whatman (Silica gel 60, 4420-222), and cut into 75 × 3 mm lanes. The silica gel layer has an internal pore size of nominally 6 nm, pore volume of 0.8 cm^3/g, and film thickness of nominally 250 μm. Stationary phase porous layers of silica gel or diatom biosilica were activated by heating at 110 °C for 50 min in an oven to remove water.

2.5. Characterization of stationary phase

Diatom biosilica and silica gel particles were ground into powder and analyzed with a Nicolet 6700 FT-IR spectrophotometer equipped with a Smart iTR Attenuated Total Reflectance (ATR) sampling accessory. FT-IR transmittance (%) spectra were acquired from 500 cm^{-1} to 4000 cm^{-1} using 125 scans per sample analysis at 4 cm^{-1} resolution.

Scanning electron microscopy (SEM) images of silica gel and frustule biosilica TLC porous layers were obtained using an FEI Quanta 600 FEG-SEM at an accelerating voltage of 5.00 kV. Porous layers were scored with a diamond-tipped glass scribe to visualize cross sectional morphologies. Prior to imaging, the porous layers were sputter-coated in gold for 35 s using a Cressington 108 auto sputter coater to provide a 9 nm gold coating. X-ray dispersive analysis (EDX) was also performed during SEM imaging for determination of elemental composition.

The stationary phase mass loading was estimated by weighing the net mass of stationary phase on the plate divided by the total surface area. The stationary phase thickness was determined from analysis of light microscopy images of the porous layer cross section. The void fraction (φ) of the silica gel and diatom biosilica layer was estimated from the amount of material deposited, the solid density of amorphous silica (2.2 g/cm^3), and the average thickness of the porous layer. The void fraction included the void space within and between the particles. Particle dimensions of the silica gel and diatom biosilica were determined by analysis of SEM images using ImageJ software. The equivalent diameter of the particles (d_p) was estimated from area and perimeter measurements.

2.6. Thin layer chromatography (TLC) experiments

The TLC developing chamber consisted of a capped 250 mL borosilicate bottle containing 15 mL of the mobile phase. A clip fixed TLC plate to a ruler that served as the reference scale. A 200 nL aliquot of analyte solution (0.79 g/L of malachite green, 0.79 g/L fast green in ethanol) was dispensed onto a given TLC plate at a sample origin distance of 5 mm. Analytes were added individually to determine migration distance and in a mixture to assess for chromatographic separation. After ethanol completely evaporated, the TLC plate was placed within the developing chamber at an inclination angle (ψ) of 70°, but the bottom of the TLC plate was initially positioned above mobile phase surface. The sealed chamber was allowed to equilibrate for 5 min to allow the mobile phase solvent vapor to fill the chamber gas space. The TLC experiment was initiated by allowing the bottom side of the stationary phase to contact the mobile phase liquid surface. All experiments were performed at room temperature (22 °C). The calculated amount of liquid retained on the stationary phase was 45 µL for the silica gel TLC layer, and 11 µL for the diatom biosilica TLC layer.

The visible mobile phase and analyte migration on the developing TLC porous layer was captured with time by digital video (1080p resolution at 30 frames per second). The solvent front migration distance (z_f), sample migration distance (z_s), and sample spot width (w_B) were estimated from this data for given image frame by ImageJ image analysis software (National Institutes of Health). The distance scale was calibrated using the reference ruler. After generating an intensity plot of the analyte spot, a Gaussian curve was fitted to the intensity map to determine z_s (distance at maximum intensity) and w_B ($4\sigma_s$). Triplicate TLC separation experiments were performed with silica gel and diatom biosilica stationary phases. On diatom biosilica, the initial spot size was 2.55 ± 0.26 mm for malachite green vs. 2.74 ± 0.21 mm for fast green (1.0 S.D., n = 3). On silica gel, the initial spot size was 1.72 ± 0.16 mm for malachite green vs. 2.00 ± 0.20 mm for fast green (1.0 S.D., n = 3). Microscopic analysis verified that the analyte spot completely penetrated the porous film.

The mobile phase viscosity (µ) was measured by a Cannon-Fenske viscometer at 22 °C (triplicate measurement). The density (ρ) was measured with a pycnometer, and the solvent surface tension (σ) was estimated by mole fraction average of known surface tension values of the pure components comprising the mobile phase at 22 °C. The molecular diffusion coefficient (D_M) of each analyte in the mobile phase solvent was estimated by the Scheibel equation at 22 °C. For solvent system 1 (9:1:1 v/v 1-butanol:ethanol:water), µ was 2.46 ± 0.015 centipoise (cP), ρ was 0.828 g/cm^3, σ was 40 dyne/cm, and D_M was $2.05{\cdot}10^{-6}$ cm^2/s for malachite green and $1.45{\cdot}10^{-6}$ cm^2/s for fast green. For solvent system 2 (5:1:2 v/v 1-butanol:acetic acid:water), µ was 2.86 ± 0.017 cP, ρ was 0.895 ± 0.0027 g/cm^3, σ was 54 dyne/cm, and D_M was $3.06{\cdot}10^{-6}$ cm^2/s for malachite green and $2.21{\cdot}10^{-6}$ cm^2/s for fast green.

2.7. Data analysis

Capillary flow of the mobile phase within the thin porous layer of silica particles (stationary phase) is described by the Lucas-Washburn wicking-flow model, where the advancing solvent front distance (z_f) varies with time (t) according to

$$z_f^2 = \frac{4\sigma}{\mu}\frac{K}{\phi R_s}t = \chi \cdot t \tag{1a}$$

or

$$z_f^2 = 2k_o d_p \frac{\sigma}{\mu}t = \chi \cdot t \tag{1b}$$

where K is permeability of capillary solvent flow through the porous layer (cm^2), R_s is the equivalent capillary radius (cm), and χ is the mobile phase flow velocity constant (cm^2/s). In Eq. (1b), k_o is a lumped parameter for the permeability (dimensionless), which includes the R_s, K, and φ terms. The key assumption of the Lucas-Washburn model is that it ignores the effect of gravity on capillary flow. The parameter χ was estimated by linear regression from the least-squares slope of z_f^2 vs. t data, and k_o was obtained from this slope. The linear velocity of the mobile phase (u) is estimated from the derivative of Eqs. (1a) and (1b))

$$u = \frac{dz_f}{dt} = \frac{\sqrt{\chi}}{2t^{1/2}} = \frac{\chi}{2z_f} \tag{2}$$

The height equivalent to a theoretical plate (H) and the number of theoretical plates (N) required to resolve a given analyte within the porous silica layer was estimated from the retention factor (R_f) for a given solute. The retention factor is defined by

$$R_f = \frac{z_s}{z_f - z_o} \tag{3}$$

where z_o is the initial position at which the analyte is added, and z_s is analyte migration distance at solvent migration front position z_f. From R_f, N and H are respectively estimated by

$$N = \frac{1}{R_f}\left(\frac{z_s}{\sigma_s}\right)^2 = 16 z_s \frac{\left(z_f - z_o\right)}{w_B^2} \tag{4}$$

and

$$H = \frac{z_f - z_o}{N} \tag{5}$$

where σ_s is Gaussian distribution associated with analyte spot position z_s, and w_B is the measured width of the analyte spot.

The modified van Deemter Equation [20] for capillary action-driven planar adsorption chromatography describes the local variation of plate height (H) with mobile phase velocity

$$H = A d_p \left(\frac{d_p}{D_M} u\right)^{1/3} + \frac{B D_M}{u} + C \frac{d_p^2}{D_M} u \tag{6}$$

In terms of solvent migration front z_f, the integral form of the van Deemter equation for the average plate height is

$$H = \frac{3}{2} A \left(\frac{d_p^4 \chi}{2 D_M}\right)^{1/3} \frac{\left(z_f^{\frac{2}{3}} - z_0^{\frac{2}{3}}\right)}{z_f - z_0} + \frac{B D_M}{\chi}\left(z_f + z_0\right) + \frac{C \chi d_p^2}{2 D_M \left(z_f - z_0\right)} \ln\left(\frac{z_f}{z_0}\right) \tag{7}$$

where d_p is the average particle diameter (cm), and A, B, and C are the Knox constants. The first term in Eqs. (6) and (7) represents eddy diffusion, and is scaled by Knox constant A; the second term represents dispersive mass transfer of the solute in the mobile phase, and is scaled by Knox constant B; the third term represents convective mass transfer resistance and is scaled by Knox constant C. Knox parameters A, B, and C were estimated by fitting plate height (H) vs.solvent migration front position (z_f) data to Eq. (7) by nonlinear, least-squares regression (Marquardt method) using Statgraphics XVI (Statpoint Technologies) software. Eqs. (1a)–(7) above were not dependent on the thickness of the stationary phase, as long as the initial analyte spot fully penetrated the porous film, which was experimentally verified.

3. Results and discussion

3.1. Characterization of TLC porous layer morphology and chemical composition

Scanning electron microscopy (SEM) images of the silica gel and diatom biosilica TLC porous layers are presented in Fig. 2. Both diatom biosilica and silica gel particles were randomly deposited on the glass substrate as a uniform, porous layer. However, SEM images revealed important structural differences between the diatom biosilica and silica gel porous layers, including particle shape, size, orientation, and packing density. The diatom biosilica frustules deposited in the porous layer were largely intact. These diatom biosilica particles were ellipsoidal in shape with a highly-porous internal structure, whereas silica gel particles possessed an irregular, granular morphology with a microporous internal pore structure.

Table 1 compares the particle properties of the TLC porous layers. For the diatom biosilica particles, the average major and minor axis lengths were 19 ± 6 (1.0 S.D., n = 158) μm by 8 ± 3 (1.0 S.D., n = 158) μm. However, the mean equivalent particle diameters (d_p) for the diatom biosilica and silica gel particles were comparable (12 vs. 10 μm). Due to their ellipsoidal shape, the diatom biosilica particles were randomly packed into the TLC porous layer more loosely relative to silica gel particles, leading to higher porosity (void fraction) and lower mass loading. The BET surface area of *Pinnularia* sp. frustules isolated by hydrogen peroxide treatment of cultured cells is reported to be 28 m^2/g [21], vs. 500 m^2/g for silica gel 60 [11]. The solid biosilica portion of *Pinnularia* sp. contains mesopores ranging from 1 to 10 nm with pore volume of 0.15–0.20 cm^3/g [21], whereas the silica gel 60 contains mesopores with an average diameter of 6 nm and pore volume of nominally 0.8 cm^3/g [11]. However, as revealed by the SEM images, the diatom biosilica frustules were hollow with a shell containing 200 nm pores on a nominal 300 nm rectangular pitch, and it was these structural features that contributed most significantly to the high porosity of 96%. SEM/EDX analysis confirmed that the elemental (atomic) composition of diatom biosilica (65.6% O, 34.4% Si) was similar that of TLC silica gel 60 (66.6% O, 33.4% Si), and did not contain any significant levels of metal impurities.

The IR spectra of the silica gel and diatom biosilica are compared in Fig. 3. Both IR spectra are characteristic of hydrated, amorphous silica. The broad peak ~3400 cm^{-1} is attributed to adsorbed water. The prominent peaks at 1069 cm^{-1}, 829 cm^{-1}, and 580 cm^{-1} are attributed to asymmetric stretching, symmetric stretching, and bending vibrations of siloxane groups. Silanol vibrations are responsible for the absorbance peak at 946 cm^{-1}. The average ratio of silanol (Si—OH) peak at 946 cm^{-1} to siloxane (Si—O—Si) peak at 1069 cm^{-1} was 0.24 for silica gel and 0.27 for diatom biosilica. It is well known that silanol groups possess enhanced acidity that affect analyte-stationary phase interactions in silica-based supports for liquid chromatography [222]. However, since both stationary phases consisted of hydrated silica rich in silanol groups of similar density, they were assumed to possess similar adsorption chemistry for a given analyte.

3.2. Comparison of flow characteristics within TLC porous layers

Solvent front migration distance (z_f) vs. time profiles for wicking flow of the mobile phase through silica gel and the diatom biosilica TLC stationary phases are presented in Fig. 4 for solvent system 1 (9:1:1 v/v 1-butanol:ethanol:water) and solvent system 2 (5:1:2 v/v 1-butanol:acetic acid:water). The rate of capillary rise decreased due to viscous effects and increasing gravitational hydrostatic pressure, leading to a monotone decreasing solvent migration front vs. time profile. The solvent front migrated more rapidly through silica gel porous layer compared to the diatom biosilica porous layer.

The data presented in Fig. 4 were fitted to the Lucas-Washburn wicking flow model (Eqs. (1a) and (1b)). Estimated flow parameters are presented in Table 1. The diatom biosilica TLC porous layer was highly porous with void fraction of 0.96, compared to 0.80 for the silica gel porous layer. For both solvent systems, the mobile phase flow velocity constant (χ) was lower for the diatom biosilica layer relative to the silica gel porous layer. The silica gel TLC porous layer flow velocity constant agreed with previously reported values [13]. Similarly, the permeability factor (k_o) was lower by a factor of two for the diatom biosilica vs. the silica gel porous layer.

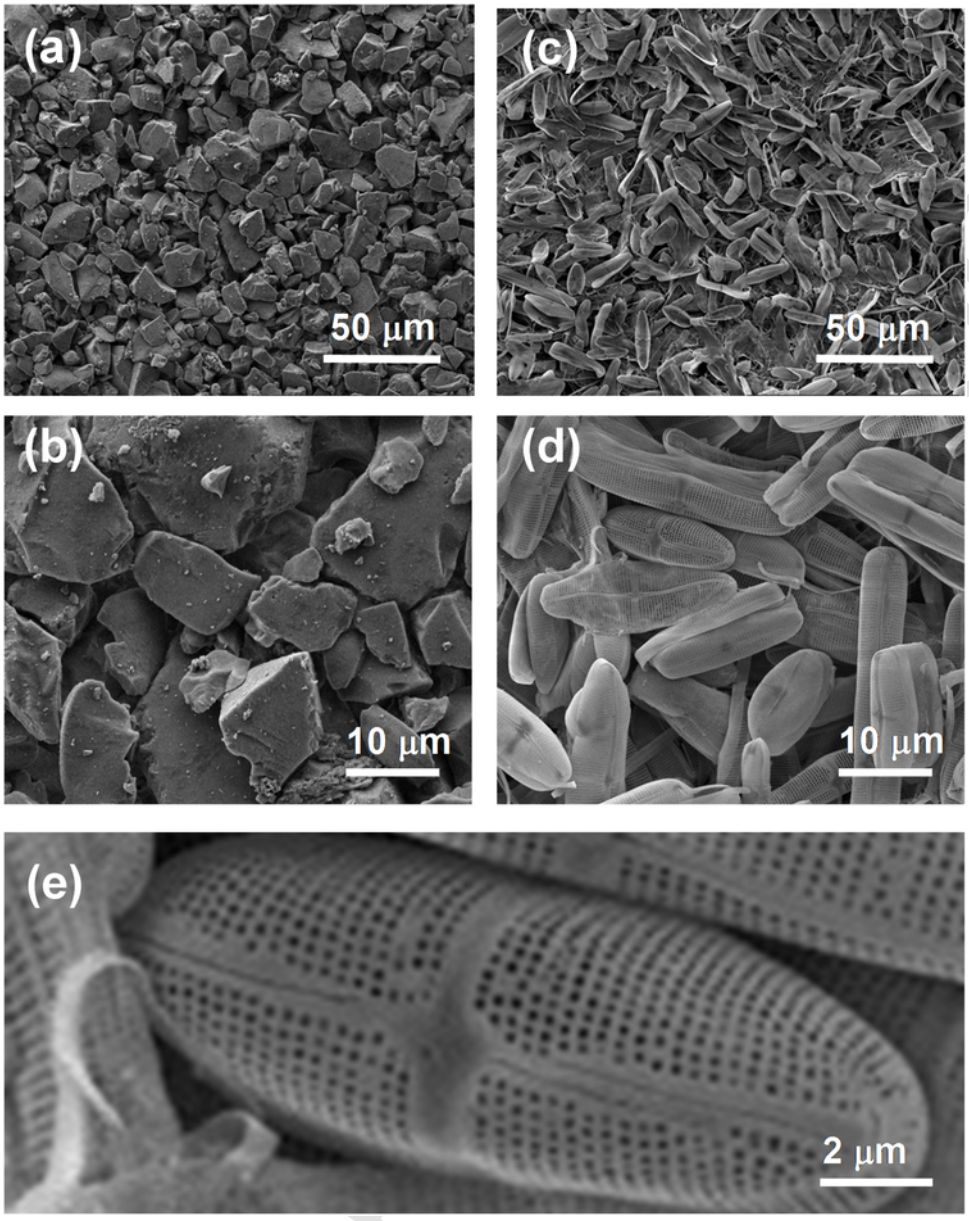

Fig. 2. SEM images of porous layers. Silica gel (a, b); diatom biosilica (c–e).

Table 1
Structure and flow properties of TLC porous layers. All reported errors are ± 1.0 S.E.

Property	Silica Gel	Diatom Biosilica
Equivalent particle diameter, d_p (μm)	10.1 ± 0.4	11.9 ± 0.2
Porous layer thickness, L (μm)	250 ± 5	53 ± 3
Stationary phase loading, m_s (μg/cm^2)	11117	500
Void fraction, ? (cm^3 void/cm^3 bulk)	0.80	0.96
Solvent system 1 velocity constant, χ (cm^2/s)	0.020 ± 0.0001	0.012 ± 0.00008
Solvent system 1 permeability constant, k_o (dimensionless)	0.0061 ± 0.0003	0.0030 ± 0.00006
Solvent system 2 velocity constant, χ (cm^2/s)	0.019 ± 0.00005	0.015 ± 0.00003
Solvent system 2 permeability constant, k_o (dimensionless)	0.0050 ± 0.0002	0.0033 ± 0.00006

3.3. TLC separation of malachite green and fast green

Malachite green is relatively nonpolar and weakly cationic with two N-dimethyl groups. In contrast, fast green has two anionic benzyl sulfonate groups, one attached to each of the amine groups, and a third anionic phenol sulfonate group (Fig. 1). Representative chromatograms in Fig. 5 demonstrate TLC separation of malachite green and fast green analytes on silica gel and diatom biosilica stationary phases. Malachite green eluted faster than fast green on both solvent system 1 (9:1:1 v/v 1-butanol:ethanol:water) and solvent system 2 (5:1:2 v/v 1-butanol:acetic acid:water) mobile phases. On silica gel, fast green did not elute when solvent system 1 was used as the mobile phase. However, the more polar mobile phase (solvent system 2) promoted migration of both phases. In contrast, diatom biosilica promoted migration of both analytes for each solvent system. Fast green

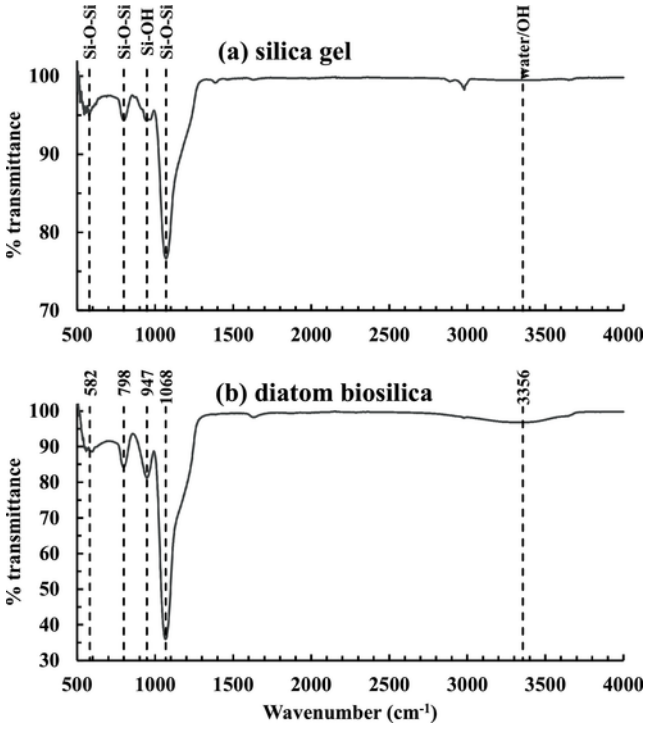

Fig. 3. FT-IR spectra of silica gel 60 and diatom biosilica.

had a lower mobility than malachite green, because the benzene and phenol sulfonate groups on fast green presumably interacted more strongly with the silanol groups.

The relative retention factor (R_f) defined by Eq. (3) did not change significantly past a solvent front migration distance of 3.0 cm. Average values of R_f for malachite green and fast green on diatom biosilica and silica gel are compared in Table 2 for solvent systems 1 and 2. The difference between R_f values for malachite green and fast green, ΔR_f, as a function of solvent front position (z_f) are presented in Fig. 6. For solvent system 1, ΔR_f values for diatom biosilica leveled off within increasing z_f, whereas ΔR_f for the silica gel layer decayed rapidly toward zero. However, for solvent system 2 ΔR_f was constant with z_f. Since fast green did not elute significantly in solvent system 1, its ΔR_f was higher relative to solvent system 2. Overall, enhanced analyte migration and complete separation resolution was observed on the diatom biosilica layer, but not on the silica gel layer. Values of R_f for both malachite green and fast green were much higher on the diatom biosilica relative to the silica gel, suggesting that both analytes were bound more strongly within the silica gel stationary phase. Silica gel has a random-mesoporous internal structure whereas diatom biosilica does not. Given the likely diffusional limitations of the analyte within the internal pores within silica gel, capillary flow velocity was not sufficient to promote separation of the two analytes on this stationary phase.

For diatom biosilica stationary phase, the R_f data shown in Fig. 6 and Table 2 were based on average values of three trials on separate TLC plates using two separately prepared samples of diatom biosilica. Analysis of Variance (ANOVA) confirmed that at z_f values greater than 3.0 cm, there was no statistically significant difference in R_f values between biosilica isolation batches at 95% confidence (malachite green, $p = 1.5 \cdot 10^{-9} < 0.05$; fast green, $p = 2.1 \cdot 10^{-3} < 0.05$).

The plate height (H) vs. solvent front (z_f) profiles for TLC separation of malachite green and fast green on diatom biosilica and silica gel for solvent systems 1 and 2 are compared in Fig. 7. Generally, the plate height (H) for malachite green and fast green eluted on diatom biosilica was minimized at solvent front position between 2.5 and 3.0 cm, whereas H for fast green eluted on silica gel always decreased with increasing z_f. Values for H at a solvent front position of 3.0 cm are compared in Table 2. Values for plate height H were much smaller for diatom biosilica relative to silica gel, pointing to higher TLC separation efficiency. For solvent system 1, H was reduced by a factor of 5 for malachite green and 3 for fast green, whereas for the more polar solvent system 2, H was reduced by a factor of nearly 17 for malachite green and 11 for fast green. In Fig. 7, at small solvent front migration distances near the beginning of the separation process, broadening of the initial analyte spot may have contributed the dispersion process, and hence affected the plate height.

The Knox constants (A, B, C) were obtained by fitting H vs. z_f data to the modified van Deemter equation (Eq. (7)) by nonlinear regression, and best-fit estimates are provided in Table 2. Best-fit esti-

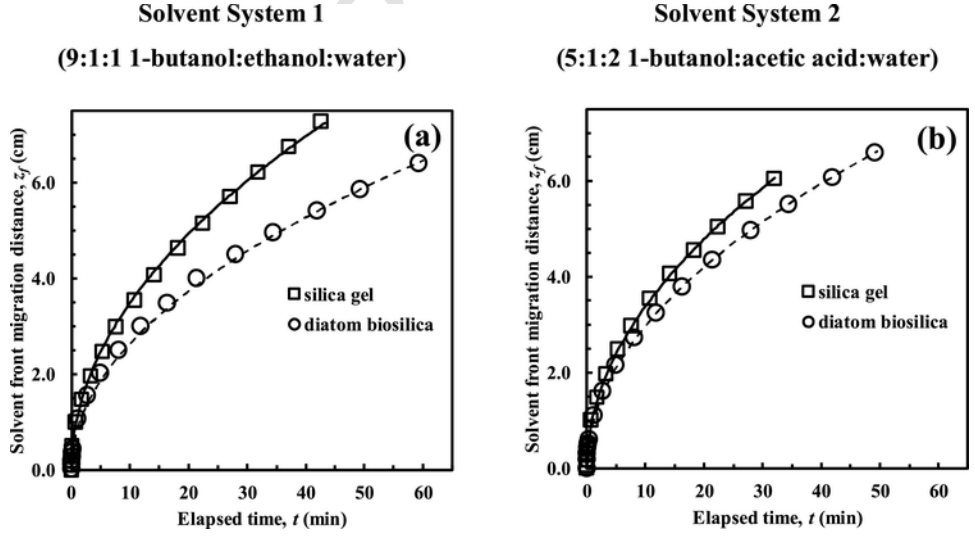

Fig. 4. Solvent front migration distance (z_f) vs. time profiles for capillary flow of mobile phase through silica gel and diatom biosilica porous layers. (a) Solvent system 1 (9:1:1 v/v 1-butanol:ethanol:water); (b) Solvent system 2 (5:1:2 v/v 1-butanol:acetic acid:water). Solid lines represent fit of data to Eqs. (1a) and (1b), fitted parameters are presented in Table 1.

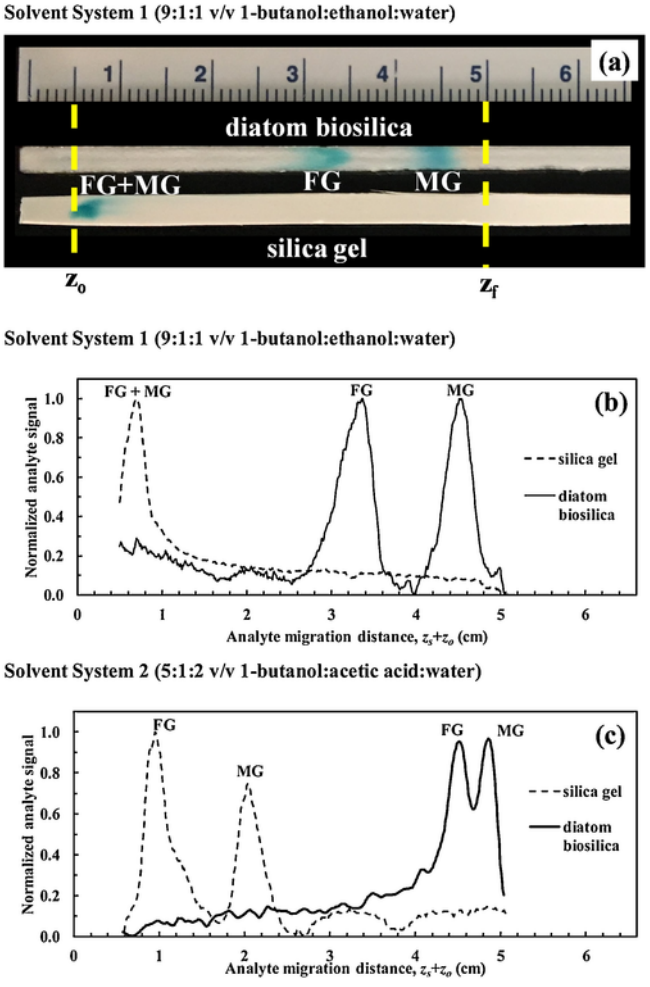

Fig. 5. TLC plates showing analyte spots for malachite green and fast green samples on diatom biosilica and silica gel after development to solvent migration front distance of z_f = 5.0 cm. (a) Photographic image, solvent system 1 (9:1:1 v/v 1-butanol:ethanol:water) (b) optical signal intensity normalized to 1.0 for highest peak, solvent system 1; (c), optical density, solvent system 2 (5:1:2 v/v 1-butanol:acetic acid:water).

mates for Knox constant A were negative or statistically zero, and so it was assumed that there was no channeling flow within the porous TLC layer. Best-fit estimates for Knox constant B, which represents dispersive mass transfer of the solute in the mobile phase, were at least 3 times higher on silica gel relative to diatom biosilica for each analyte. Best-fit estimates for the Knox constant C, which represents convective mass transfer resistance of the solute between the mobile and stationary phases, were also at least 3 times higher for silica gel relative to diatom biosilica for each analyte.

3.4. Basis for improved separation of malachite green and fast green on diatom biosilica

This study has shown that a thin porous layer for conventional TLC composed of diatom biosilica significantly improved the separation of the triphenylmethane dyes malachite green and fast green relative to silica gel. The results suggest that basis for improved separation is the unique nano- and microstructure of the diatom biosilica thin porous layer, which consists of randomly deposited, ellipsoidal biosilica frustules isolated from cultured cells of the pennate diatom *Pinnularia*.

Relative to the silica gel porous layer, the diatom biosilica porous layer possessed an open structure both between and within the particles with void fraction of 0.96. Each biosilica frustule possessed a uniform array of 200 nm pores penetrating through the shell (Fig. 2e). However, even with this open structure, the permeability factor for capillary flow was two times lower through diatom biosilica relative to silica gel. This result suggested the structure of the diatom biosilica promoted interaction of the mobile phase with the surface of the stationary phase. The increased interaction between the stationary and mobile phase on the diatom biosilica increased the mobility of both malachite and fast green, enabling the chromatographic resolution of these molecules. This result was observed for both solvent systems 1 and 2.

The use of diatom biosilica significantly lowered the minimum plate height relative to silica gel for each analyte, suggesting that the diatom biosilica porous layer offered enhanced mass transfer relative to the silica gel porous layer. The six-fold decrease in Knox constant B for malachite green reflects a reduction in dispersive mass transfer. The structure of the diatom biosilica offers an open structure with lowered intraparticle diffusion resistance relative to microporous silica gel. Furthermore, the nearly three-fold decrease in Knox constant C for both analytes reflects a reduction of the convective mass transfer resistance for solute transfer from the mobile phase to the particle surface. The surface of diatom silica frustules is corrugated with a rectangular array of 200 nm pores. This surface topology would help disrupt the fluid boundary layer surrounding the particle, resulting in an improved convective mass transfer rate.

In conventional porous particle layers for TLC, capillary forces cannot generate sufficient flow to minimize the effects of zone broadening [1], and silica gel particle layers in particular suffer from inadequate mass transfer [13]. Monolithic stationary phases for TLC with open internal pore structure offer improvements in performance [23].

Table 2
TLC parameters for separation of malachite green and fast green on silica gel and diatom biosilica stationary phases.

	Malachite Green		Fast Green	
TLC Parameter	Silica Gel	Diatom Biosilica	Silica Gel	Diatom Biosilica
Solvent System 1 (9:1:1 v/v 1-butanol:ethanol:water)				
Knox Constant B (± 1.0 S.E.)	36 ± 8.3	6.2 ± 1.2	57 ± 19	3.4 ± 2.2
Knox Constant C (± 1.0 S.E.)	4.4 ± 1.9	1.5 ± 0.7	16 ± 2.2	6.4 ± 0.6
Plate height H at z_f = 3 cm (μm)	345 ± 51	70 ± 5.9	432 ± 60	152 ± 27
R_f ($z_f \geq$ 3.0 cm)	0.109 ± 0.019	0.774 ± 0.007	0.083 ± 0.004	0.511 ± 0.009
Solvent System 2 (5:1:2 v/v 1-butanol:acetic acid:water)				
Knox Constant B (± 1.0 S.E.)	157 ± 19	9.0 ± 0.9	35 ± 27.2	14 ± 3.1
Knox Constant C (± 1.0 S.E.)	92 ± 9.0	2.9 ± 0.6	37 ± 7.0	5.0 ± 1.0
Plate height H at z_f = 3 cm (μm)	348 ± 74	20 ± 5.7	435 ± 88	38 ± 8.3
R_f ($z_f \geq$ 3.0 cm)	0.311 ± 0.010	0.942 ± 0.005	0.100 ± 0.007	0.875 ± 0.008

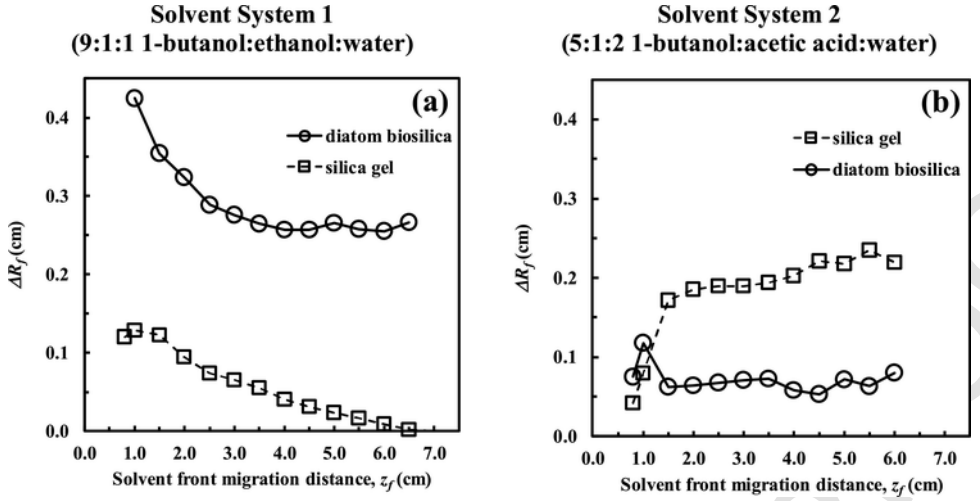

Fig. 6. Relative difference in retention factor (ΔR_f) between malachite green and fast green vs. solvent front migration distance (z_f) on silica gel and diatom biosilica porous layers. (a) Solvent system 1 (9:1:1 v/v 1-butanol:ethanol:water), average (± 1.0 S.D., n = 7) $\Delta R_f = 0.262 \pm 0.007$ (diatom biosilica), $\Delta R_f = 0.027 \pm 0.023$ (silica gel); (b) solvent system 2 (5:1:2 v/v 1-butanol:acetic acid:water), $\Delta R_f = 0.067 \pm 0.009$ (diatom biosilica), $\Delta R_f = 0.211 \pm 0.016$ (silica gel).

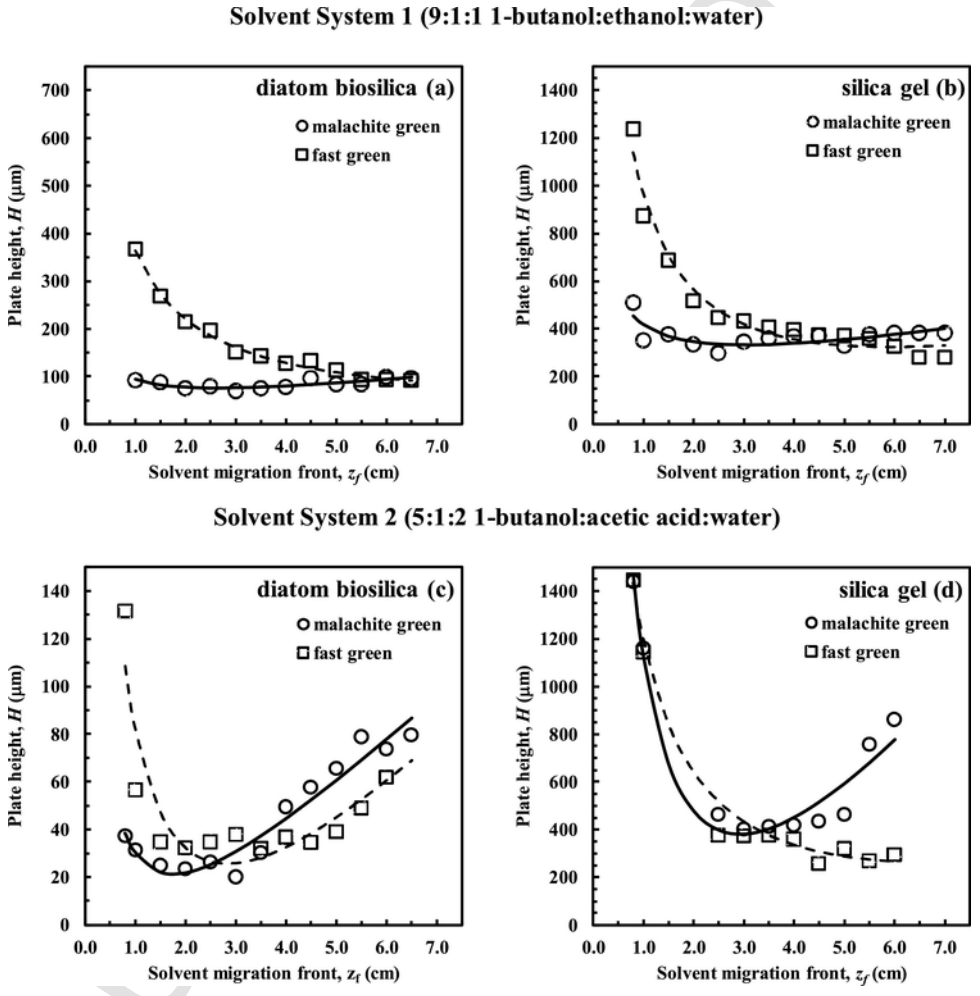

Fig. 7. Plate height (H) for separation of malachite green and fast green on silica gel and diatom biosilica. (a) Diatom biosilica, solvent sys (9:1:1 v/v 1-butanol:ethanol:water); (b) Silica gel, solvent system 1; (c) Diatom biosilica, solvent system 2 (5:1:2: v/v 1-butanol:acetic acid:water); (d) Silica gel, solvent system 2.

In this context, the ordered pore array structure on the diatom frustule surface may promote mobile phase interactions with the stationary phase, leading to improved mass transfer and analyte resolution.

Previous work has used atomic layer deposition (ALD), plasma-enhanced chemical vapor deposition (PECVD), physical vapor deposition, and electrospinning to create nanostructured, silica-based thin films for ultra TLC [7–9,24-26]. Both ALD [7,24,25] and PECVD [26] can precisely modify the stationary phase structure to enhance analyte mobility. Furthermore, ordered microstructures facilitate convective mass transfer, leading to enhanced TLC efficiency [26]. However, these stationary phases were made through elaborate, top-down planar fabrication processes. The nanostructured diatom biosilica described in this study can be readily produced at scale through a cell cultivation process followed by chemical isolation of the diatom frustules [18]. A simple drop-casting technique is then used to deposit a thin porous layer of diatom frustules suitable for TLC.

4. Conclusions

This study showed that a stationary phase for conventional TLC composed of randomly-deposited biosilica frustules isolated from living cells of diatom *Pinnularia* sp. significantly improved the separation performance of the triphenylmethane dyes malachite green and fast green relative to silica gel. The diatom frustules were highly porous, hollow shells with surface structure dominated by 200 nm pore arrays. The migration and separation of malachite green, a relatively nonpolar, weakly cationic molecule, and fast green, a more polar, anionic molecule, could be fully separated on the open structure of diatom biosilica for both solvent systems. However, silica gel, which possessed micropores of 6 nm diameter, did not enable the migration of fast green in solvent system 1. Improved TLC performance was also reflected reduced plate height for both analytes, particularly for the more polar solvent system 2. Further chromatographic mass transfer analysis suggested that nanostructured surface of the frustule decreased boundary layer resistance and reduced dispersive mass transfer, leading to increased analyte flux. Overall, these analyses suggest that the basis for improved chromatographic performance is the unique nano- and microstructure of the diatom biosilica frustule. Therefore, nanostructured diatom biosilica frustules produced through cell culture of living diatom cells merit continued investigation as a new stationary phase for TLC.

Acknowledgements

This work was supported by U.S. National Science Foundation (grant numbers 1701329 and 1240488), and the U.S. Department of Agriculture (grant number 2017-67021-26606).

References

[1] C.F. Poole, Thin-layer chromatography: challenges and opportunities, J. Chromatogr. A 1000 (2003) 963–984, https://doi.org/10.1016/S0021-9673(03)00435-7.
[2] F. Rabel, J. Sherma, Review of the state of the art of preparative thin-layer chromatography, J. Liq. Chromatogr. Relat. Technol. 40 (2017) 165–176, https://doi.org/10.1080/10826076.2017.1294081.
[3] F. Rabel, J. Sherma, R.E. Majors, Stationary phases for modern thin-layer chromatography, LCGC N. Am. 30 (2012) 458–472.
[4] S.K. Poole, C.F. Poole, High performance stationary phases for planar chromatography, J. Chromatogr. A 1218 (2011) 2648–2660, https://doi.org/10.1016/j.chroma.2010.10.072.
[5] T.H. Jupille, J.A. Perry, High-performance thin-layer chromatography: a review of principles, practice, and potential, Crit. Rev. Anal. Chem. 6 (1977) 325–359, https://doi.org/10.1080/10408347708085696.
[6] L.W. Bezuidenhout, M.J. Brett, Ultrathin layer chromatography on nanostructured thin films, J. Chromatogr. A 1183 (2008) 179–185, https://doi.org/10.1016/j.chroma.2007.12.089.
[7] S.R. Jim, A. Foroughi-Abari, K.M. Krause, P. Li, M. Kupsta, M.T. Taschuk, K.C. Cadien, M.J. Brett, Ultrathin-layer chromatography nanostructures modified by atomic layer deposition, J. Chromatogr. A 1299 (2013) 118–125, https://doi.org/10.1016/j.chroma.2013.05.050.
[8] J. Wannenmacher, S.R. Jim, M.T. Taschuk, M.J. Brett, G.E. Morlock, Ultra-thin-layer chromatography on SiO_2, Al_2O_3, TiO_2, and ZrO_2 nanostructured thin films, J. Chromatogr. A 1318 (2013) 234–243, https://doi.org/10.1016/j.chroma.2013.09.083.
[9] T.E. Newsome, S.V. Olesik, Silica-based nanofibers for electrospun ultra-thin layer chromatography, J. Chromatogr. A 1364 (2014) 261–270, https://doi.org/10.1016/j.chroma.2014.08.065.
[10] G.L. Rorrer, Chapter 4: functionalization of frustules from diatom cell culture for optoelectronic properties, in: D. Losic (Ed.), Diatom Nanotechnol. Prog. Emerg. Appl., Royal Society of Chemistry, 2018, pp. 79–110, https://doi.org/10.1039/9781788010160-00079.
[11] S. Gocan, Stationary phases for thin-layer chromatography, J. Chromatogr. Sci. 40 (2002) 538–549, https://doi.org/10.1093/chromsci/40.10.538.
[12] K. Sednev, V. Berezkin, Thin-layer chromatography of polar and ionic compounds using active gas flow over the silica gel adsorbent layer, J. Planar Chromatogr. – Mod. TLC24 (2011) 181–187, https://doi.org/10.1556/JPC.24.2011.3.1.
[13] C.F. Poole, W.P.N. Fernando, Some musings on the measurement and interpretation of theoretical plate height in thin-layer chromatography, J. Planar Chromatogr. 5 (1992) 323–333.
[14] S. Srivastava, R. Sinha, D. Roy, Toxicological effects of malachite green, Aquat. Toxicol. 66 (2004) 319–329, https://doi.org/10.1016/j.aquatox.2003.09.008.
[15] N. López-Gutiérrez, R. Romero-González, J.L. Martínez Vidal, A.G. Frenich, Analysis of triphenylmethane dyes in seafood products: a review of extraction methods and determination by liquid chromatography coupled to mass spectrometry, Anal. Methods5 (2013) 3434–3449, https://doi.org/10.1039/c3ay40485d.
[16] P.E. Wall, The value of planar chromatography for the analysis of triphenylmethane dyes, J. Planar Chromatogr. 6 (1993) 394–403.
[17] P.E. Wall, Dyes | Thin-layer (planar) chromatography, in: I.D. Wilson (Ed.), Encylopedia Sep. Sci., Academic Press, Cambridge, 2000, pp. 2619–2631, https://doi.org/10.1016/B0-12-226770-2/02701-0.
[18] C. Jeffryes, T. Gutu, J. Jiao, G.L. Rorrer, Two-stage photobioreactor process for the metabolic insertion of nanostructured germanium into the silica microstructure of the diatom Pinnularia sp, Mater. Sci. Eng. C28 (2008) 107–118, https://doi.org/10.1016/j.msec.2007.01.002.
[19] J.A. Berges, D.J. Franklin, P.J. Harrison, Evolution of an artificial seawater medium: improvements in enriched seawater, artificial water over the last two decades, J. Phycol. 37 (2001) 1138–1145, https://doi.org/10.1046/j.1529-8817.2001.01052.x.
[20] B. Spangenberg, C.F. Poole, C. Weins, Theoretical basis of thin layer chromatography (TLC), in: B. Spangenberg (Ed.), Quant. Thin-Layer Chromatogr., Springer, Berlin Heidelberg, Berlin, Heidelberg, 2010, pp. 13–52, https://doi.org/10.1007/978-3-642-10729-0_2.
[21] E. Van Eynde, B. Lenaerts, T. Tytgat, S.W. Verbruggen, Effect of pretreatment and temperature on the properties of Pinnularia biosilica frustules, RSC Adv. 4 (2014) 56200–56206,https://doi.org/10.1039/C4RA09305D.
()
[22] J. Nawrocki, The silanol group and its role in liquid chromatography, J. Chromatogr. A779 (1997) 29–71.
[23] F.C. Leinweber, U. Tallarek, Chromatographic performance of monolithic and particulate stationary phases, J. Chromatogr. A 1006 (2003) 207–228, https://doi.org/10.1016/S0021-9673(03)00391-1.
[24] A.J. Oko, S.R. Jim, M.T. Taschuk, M.J. Brett, Analyte migration in anisotropic nanostructured ultrathin-layer chromatography media, J. Chromatogr. A 1218 (2011) 2661–2667, https://doi.org/10.1016/j.chroma.2010.12.021.
[25] S.R. Jim, A.J. Oko, M.T. Taschuk, M.J. Brett, Morphological modification of nanostructured ultrathin-layer chromatography stationary phases, J. Chromatogr. A 1218 (2011) 7203–7210, https://doi.org/10.1016/j.chroma.2011.08.024.
[26] N.A. Crane, N.V. Lavrik, M.J. Sepaniak, Manipulating the inter pillar gap in pillar array ultra-thin layer planar chromatography platforms, Analyst141 (2016) 1239–1245, https://doi.org/10.1039/c5an02274f.